Plasticity induced crack closure during fatigue crack propagation: numerical prediction of the crack front shape in 304L stainless steel

W. Taleb[a], C. Gardin[a], C. Sarrazin-Baudoux[a]

a. Institut Pprime, Téléport 2, 1 avenue Clément Ader, 86961 Futuroscope Chasseneuil, France

wissam.taleb@ensma.fr

Abstract:

The objective of this study is to investigate the fatigue crack propagation through numerical simulations while considering the effect of the plasticity induced closure. A straight crack front is initiated in a compact tension CT specimen made of 304L stainless steel. The specimen is then loaded at a constant stress intensity factor amplitude in order to eliminate the influence of the loading history. The propagation of the crack is driven by the effective stress intensity factor amplitude ΔK_{eff} which is calculated after parallel elastic and plastic independent simulations. The elastic simulation is used to evaluate the maximum stress intensity factor K_{max} using the crack tip stress field method while the opening stress intensity factor K_{op} is evaluated after the plastic one. An automatic remeshing procedure is also used to respond to the geometrical changes in the model after the crack propagation. The numerical results are compared with previously conducted experiments and show a globally good accordance.

Résumé:

L'objectif de cette étude est d'étudier la propagation des fissures de fatigue par des simulations numériques en tenant compte de l'effet de la fermeture induite par la plasticité. Un front droit de fissure est initié dans une éprouvette CT compacte en acier inoxydable 304L. L'éprouvette est ensuite sollicitée en fatigue avec une amplitude de facteur d'intensité de contrainte constante afin d'éliminer l'influence de l'historique de chargement. La propagation de la fissure est déterminée par l'amplitude du facteur d'intensité de contraintes effective ΔK_{eff}, calculée à l'aide de simulations parallèles élastiques et plastique indépendantes. La simulation élastique permet d'évaluer le facteur d'intensité de contraintes maximum K_{max} à l'aide de la méthode des champs de contrainte en pointe de fissure, tandis que la simulation plastique donne le facteur d'intensité de contraintes à l'ouverture K_{op}. Une procédure de remaillage automatique est également utilisée pour répondre aux modifications géométriques du modèle après chaque relâchement des nœuds. Les résultats numériques sont comparés aux expériences menées précédemment et montrent une bonne concordance globale.

Keywords: 3D numerical calculations, fatigue crack propagation, crack front shape, plasticity induced crack closure.

1 Introduction

The study of the reliability of structures has always drawn the attention of researchers due to its significance and to the serious consequences that it may lead to, unless carefully addressed. The fatigue phenomenon is classified as the most important and most frequent provoker for the structure's damage. For that reason, scientists invested a lot of time to understand the influence of fatigue on crack propagation and then to integrate it into models that can simulate the reality.

In the past, because of limitations in calculation resources, most of the first models were simulated in a two dimensional approach [1], mainly under the assumption of linear elastic fracture mechanics. More recently, 3D effects were considered [2–4].

Considered as one of the most important 3D effects to be studied, the Plasticity Induced Crack Closure (abbreviated PICC) is a phenomenon discovered by Elber [5] in the 1970's : during fatigue loading, compressive residual stresses develop in the plastic wake ahead of the crack tip and affect the value of the load corresponding to contact between the crack lips, load corresponding to the opening stress intensity factor K_{op}. The resulting effective portion of the stress intensity factor amplitude, considered as the driving force [6,7], is then $\Delta K_{eff} = K_{max} - K_{op}$.

An accurate propagation of a crack in a 3D model has to consider that the geometry of the crack front is changing up to a stabilized shape: in this aim, some authors [8–10] used the method of adaptive remeshing. Sometimes, predefined shapes, often semi elliptical, have been assigned to the various crack fronts.

Finally, it is crucial also to invest in the precision of the calculation of the stress intensity factors. Many methods were used in the literature: J integral and energetic methods, or interpolation of the stress or displacement fields. In a previous study, Fiordalisi [11] demonstrated that the Shih and Asaro method implemented in ABAQUS does not allow to represent accurately edge effects.

So, this paper will present a fatigue crack propagation 3D model based on a calculation of the stress intensity factors based on an interpolation of the stresses, while taking into account the influence of the plasticity induced crack closure.

2 Numerical model

The geometry of the specimen studied is a standard CT-50 compact specimen with a thickness of 10mm.For reasons of symmetry, only a quarter of the specimen is modeled as illustrated in Figure 1a. The initial crack front is straight.

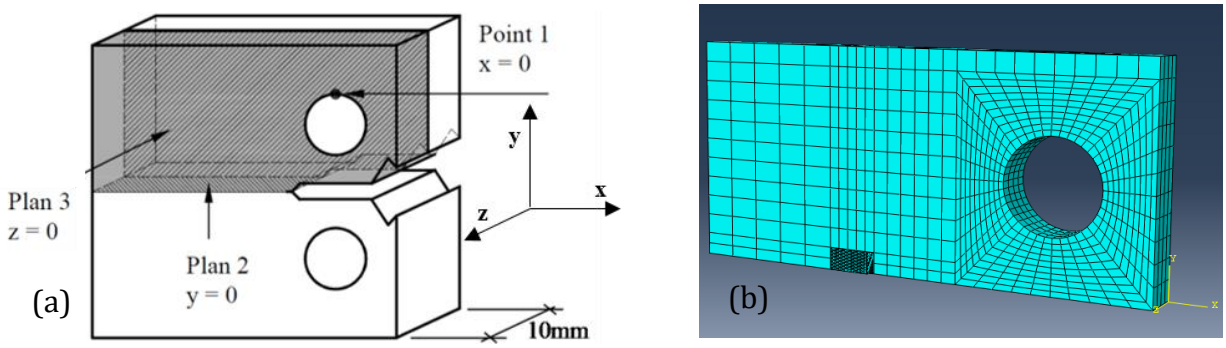

Figure 1: (a) Geometry of the CT specimen used and the symmetry planes (b) Mesh scheme used

The model is loaded under pure mode I with a constant amplitude of the stress intensity factor $\Delta K=12MPa\sqrt{m}$ and a load ratio R=0.1 to ensure the presence of plasticity induced crack closure. The load is represented by applying cyclic pressure on a quarter of the hole along the y direction.

The body is divided into two parts, meshed with different number of elements as shown in Figure 1b. The part close to the crack tip, which is affected with high stress gradients is highly refined, the rest of the mesh is coarse. Dougherty et al. [12] recommended the use of at least 10 elements in the monotonic plastic zone R_p near the crack tip in the direction of propagation. In our case, and in order to insure better reliability of our results, 20 elements are used. Their dimension along the direction of propagation is equal to 0.1 mm. Along the thickness, 20 elements are also used: their size gradually decreases from the center towards the edge, respecting the recommendations of Roychowdhury and Dodds [3]. Eight-node linear and fully integrated brick elements, C3D8, are used all over the body mesh. The plasticity-induced crack closure is modelled by the contact of the crack flanks which is interpreted as the frictionless contact of one analytical rigid surface and the simulated crack plane.

The isotropic and kinematic constitutive law (Table 1), considered for 304L stainless steel, required a large number of cycles to reach a steady state of the stress and strain fields near the crack tip. To answer this problem, a balance between the number of cycles between each release and the computational time is considered to be optimised with 5 cycles [10].

Elasticity		Kinematic hardening			Isotropic hardening		
E [MPa]	ν	σ_0 [MPa]	C [MPa]	D	σ_0 [MPa]	Q [MPa]	b
196000	0.3	117	52800	300	117	87	9

Table 1: Parameters of the constitutive law for the 304L stainless steel studied [11].

3 Methodology

3.1 Calculation of the stress intensity factors

The calculation of the stress intensity factor SIF is generally limited to two main approaches:

- The first approach is based on the calculation of energy via the J-integral. Nevertheless, in a previous study, Fiordalisi [11] demonstrated that the Shih and Asaro method implemented in ABAQUS does not allow to represent accurately edge effects.
- The other is based on the interpolation of stresses or displacements in the vicinity of the crack tip. The calculation of the SIF through strain fields imposes an assumption concerning the evolution of the state of stress throughout the specimen thickness (plane strain vs plane stress). Thus it is not easy to implement it in a three dimensional approach as it remains a very controversial subject.

As a consequence, the method of stress fields is used here since it does not require any prior assumption concerning the stress state along the thickness.

Following linear elastic fracture mechanics, the relation between the SIF and the stresses in mode I is the following:

$$\sigma_{ij} = \frac{K_I}{\sqrt{2\pi r}} f_{ij}(\theta) + higher\ order\ terms \quad (1)$$

where σ_{ij} is the stress tensor, r and θ are the polar coordinates, and fij is a dimensionless function depending on the angular position θ, the loading mode and the geometry of the part.

For simplification matters, the stress perpendicular to the crack propagation plane σ_{yy} is only extracted for the nodes on the axis of symmetry (θ = 0). Equation 1 is then simplified as follows:

$$\sigma_{yy} = K_I \left(\frac{1}{\sqrt{2\pi r}}\right) \quad (2)$$

The stress intensity factor K_I is then the slope of the curve σ_{yy} versus (1 / √2πr), as shown in Figure 2. A PYTHON script has been specifically implemented in that aim.

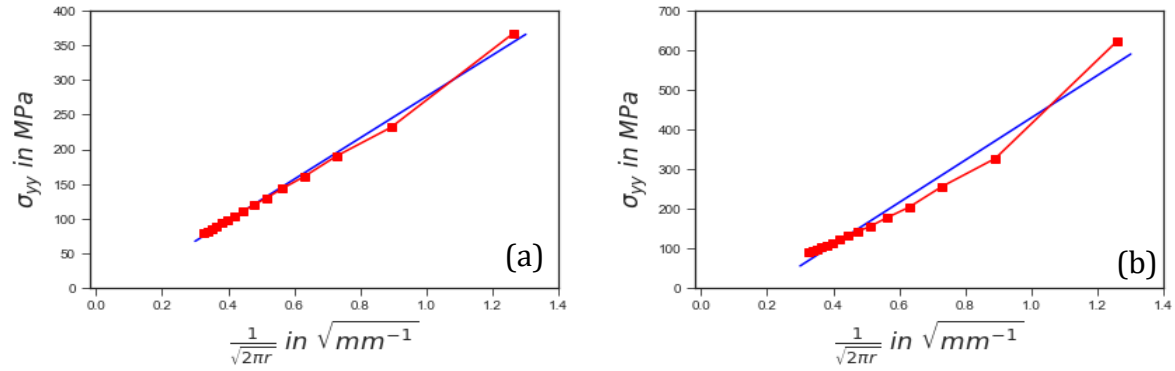

Figure 2: interpolation of the values of K using the stresses at the crack tip ΔK=12MPa√m, R=0.1, edge's node (a) First iteration (b) after 15 iterations

The number of nodes used in this interpolation, in addition to their position with respect to the crack front, are also critical because of the various parameters that affect the stress calculation, as the mesh and the proximity to the crack. After several attempts, we have finally chosen to retain the 15 closest nodes to the crack front for the interpolation in such a way to consider a large number of nodes, without exceeding the limits of the SIF consistency zone, even if the value for the closest node (highest value here of (1 / √2πr)) changes in an important way the value of K.

3.2 Method presentation

The procedure followed in the propagation of the crack is presented below:

a) The initial numerical model is prepared as explained in paragraph 2,

b) Two parallel simulations are launched:

- An elastic simulation allowing to obtain the values of the local maximum stress intensity factor K_{max}^{ℓ} at each node of the crack front,
- A plastic simulation for the calculation of the local opening stress intensity loads corresponding to the loss of contact P_{op}^{ℓ}. Then we assume that:

$$K_{op}^{\ell} = K_{max}^{\ell} \frac{P_{op}}{P_{max}} \quad (3)$$

The effective local stress intensity factor amplitude K_{eff}^{ℓ} is then calculated as follows:

$$\Delta K_{eff}^{\ell} = \Delta K_{max}^{\ell} - \Delta K_{op}^{\ell} \quad (4)$$

c) The advancement at each node over the thickness is calculated by using the equation proposed by Lin and smith [13] :

$$\Delta a_i = \left(\frac{\Delta K_{eff,i}^{\ell}}{\Delta K_{eff,max}^{\ell}} \right)^m \Delta a_{max} \quad (5)$$

where m is the Paris law exponent, $\Delta K_{eff,max}^{\ell}$ is the maximum effective stress intensity factor along the crack front, and Δa_{max} is the maximum advancement allowed, chosen to be 0.1mm at the node where ΔK_{eff}^{ℓ} is the highest, in a compromise between accuracy and the simulation duration,

d) The advancements are fit in a semi elliptical-like crack front which is then integrated as a new front in the body geometry,
e) The part concerned with the geometry update is then remeshed to respond to the new changes,
f) The same procedure is repeated over and over until the stabilization criterion is reached.

3.3 Interpolation of the crack front in a semi-elliptical shape

The values of the crack advances Δa_i obtained in all the nodes along the crack front are interpolated using a semi-elliptical predefined shape. This mathematical assumption allows to fit the experimental results obtained by Arzaghi et al. [14] and Fiordalisi [11], and is widely used in the literature by many other authors [15–19].

PYTHON was also used here to interpolate the crack advance values using a Gauss Newton nonlinear interpolation function specifically developed in this purpose. Only one half of the ellipse is interpolated as a result of symmetry and its center is considered to be in the middle of the initial crack front as shown in Figure 3.

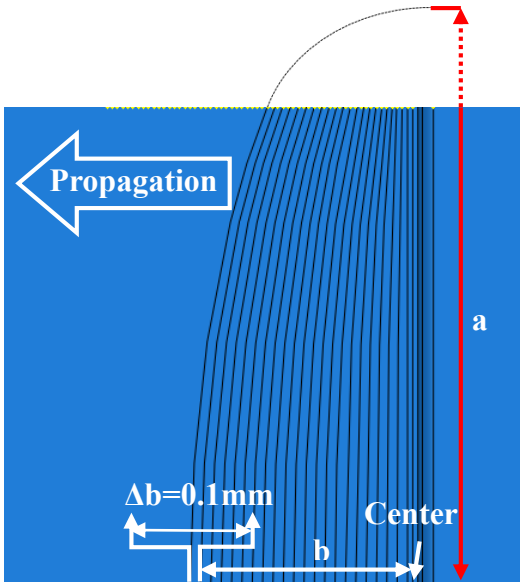

Figure 3 : Predefined semi elliptical crack front shape

3.4 Remeshing

The technique of adaptive remeshing is used to readjust the mesh to the new geometry changes according to the results of the previous calculation. In our case, the crack front evolves from a straight form to a semi-elliptical one, therefore, updating the mesh at each release is essential.

The new interpolated semi elliptical crack front is integrated into the geometry as a partition. The mesh is then updated to maintain the newly created geometry of the crack front. The technique has the advantage of following the growth of the crack without any predefined assumption.

It is shown that, during the propagation of the crack, the various nodes along the crack front tend to get closer to the edge of the specimen because of the increase in the front curvature. Therefore, another function was developed in PYTHON to align the cascading nodes at the same abscissa z because these nodes are used to interpolate SIF and must share the same level. This is illustrated in Figure 4.

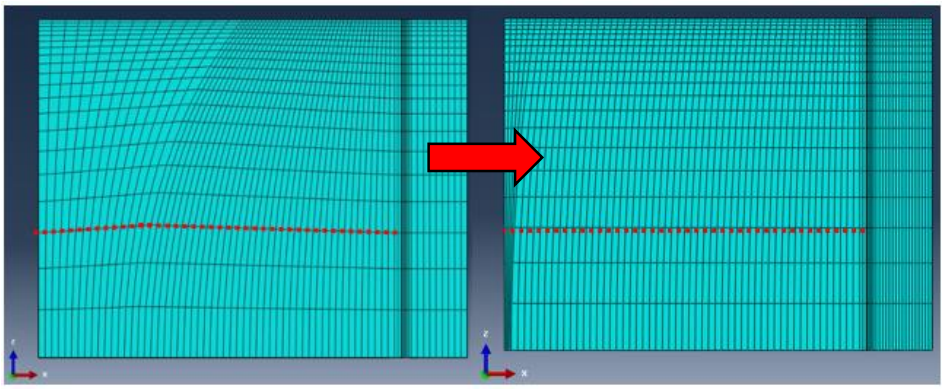

Figure 4: mesh alignment after each propagation

3.5 Stabilization criterion

As explained previously, several steps of numerical calculation have to be made in order to follow the crack shape evolution. It is thus necessary to define a stabilization criterion to determine the final crack front.

Here, two stabilization criteria are compared.The first, denoted relative error E_{rel} in Equation 6, corresponds to the percentage ratio of the difference between ΔK_{eff}^{ℓ} at the center of the CT specimen and that at the edge, over the maximum value of ΔK_{eff}^{ℓ} along the crack front $\Delta K_{eff,max}^{\ell}$ .On the other hand, the second stabilization method, absolute error E_{abs} in Equation 7, corresponds to the percentage ratio of the difference between the maximum and the minimum ΔK_{eff}^{ℓ} values, over $\Delta K_{eff,max}^{\ell}$.

$$E_{rel} = \frac{abs(\Delta K_{eff,center}^{\ell} - \Delta K_{eff,\text{edge}}^{\ell})}{\Delta K_{eff,max}^{l}} * 100 \quad (6)$$

$$E_{abs} = \frac{\Delta K_{eff,max}^{\ell} - \Delta K_{eff,\text{min}}^{\ell}}{\Delta K_{eff,max}^{\ell}} * 100 \quad (7)$$

The stabilized front is then assumed to be reached when the value of E_{rel} or E_{abs} becomes minimum. These two criteria will be compared and discussed later in this paper.

4 Comparison between numerical and experimental results

4.1 Evolution of the local effective stress intensity factor amplitude along the specimen thickness

The stress intensity factor amplitude ΔK_{eff}^{ℓ} is defined as the difference between the maximum and the opening stress intensity factors. For that purpose, the behavior of these two SIFs should be first observed. In Figure 5a, the evolution of K_{max}^{ℓ} at 6 different steps of the crack propagation are plotted: the initial step, three intermediate ones and the two final steps corresponding to the retained stabilization criteria. For the same steps, the values describing the crack closure rate are also presented in Figure 5b. The crack closure rate is an indicator for the presence of PICC and is defined as the ratio of the effective SIF amplitude over difference between the maximum and the minimum one as in equation 8:

$$U = \frac{\Delta K_{eff}^{\ell}}{K_{max}^{\ell} - K_{min}^{\ell}} \tag{8}$$

The evolution of 1-U will be plotted, in Figure 5b, to align the value of zero with the absence of PICC.

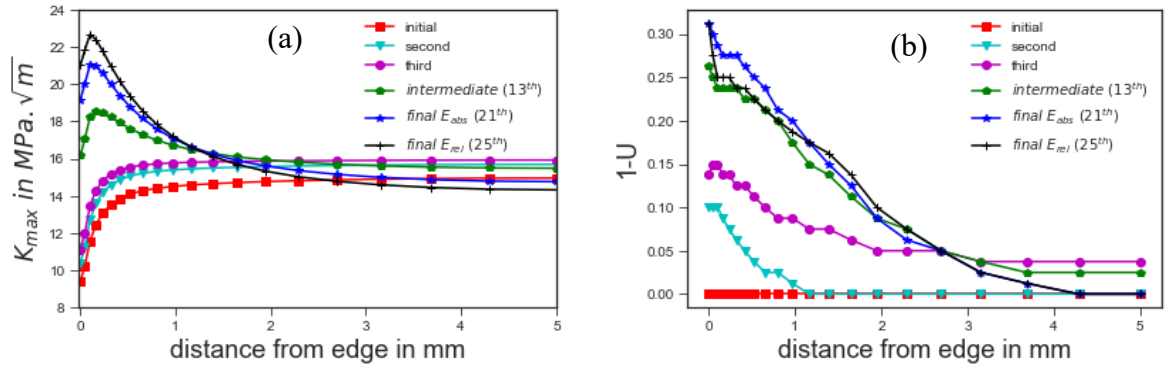

Figure 5 : evolution along the specimen thickness of (a) the local maximum stress intensity factor for the initial, intermediate and 2 final iterations (b) the crack closure rate for different steps of crack propagation

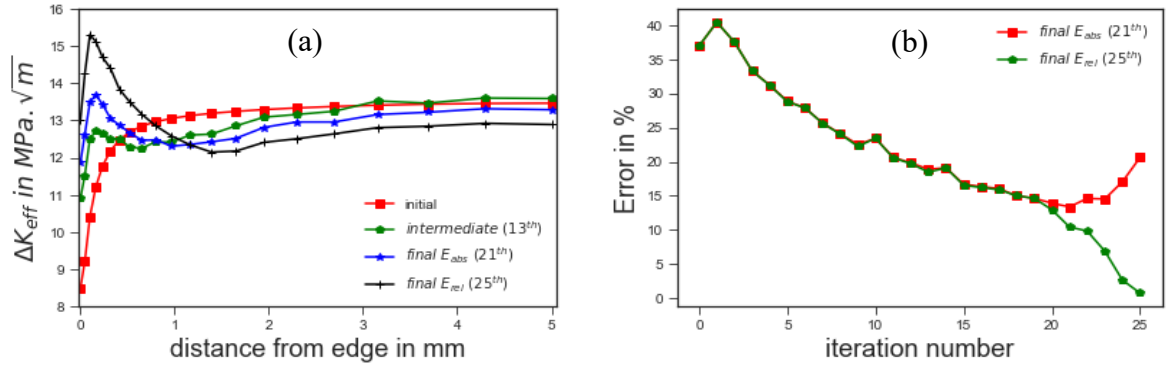

Figure 6: evolution of (a) the local effective stress intensity factor in the specimen thickness for the initial, intermediate and 2 final iterations (b) the error associated to the 2 stabilization criteria

For the initial step with a straight crack front, a large difference can be observed between the value of K_{max}^{ℓ} at the edge and that at the center. As the crack advances, it can be remarked that, at the edge, the values of K_{max}^{ℓ} tend to increase to get closer to that of the center which remains almost constant. An emergent hump on the curve can be also observed in the area close to the edge after several numbers of iterations.

In Figure 5b, it can be observed that, for the initial step, there is no crack closure along the whole specimen thickness. No plastic wake has been created, so the corresponding behavior corresponds to that of a short crack undergoing no closure. PICC then appears at the edge from the second step, and the level of closure increases up to a stabilized value (around 30% of closure) from approximately 13 steps. In the center of the specimen, almost no closure is observed, during the whole propagation. These results have been also monitored by many other authors [20].

The behavior of ΔK_{eff}^{ℓ}, shown in Figure 6a, also resembles that of K_{max}^{ℓ} with a value at the edge initially smaller than at the center, and with an increase of this edge value during the propagation, up to the curves corresponding to the stabilization criteria. When comparing the effective SIF curves corresponding to the two stabilization criteria, it can be observed that, in both cases, the values don't verify an iso-ΔK_{eff}^{ℓ} curve over the thickness, as an emergent hump is present on the curves near the specimen edges, which is larger for the relative stabilization criterion. Previous calculations by Fiordalisi [11] demonstrated also such a hump. This may raise the question on the reliability of assuming of a semi elliptical shape for the crack front which may be the origin of this hump. In this frame, it would be much interesting to implement propagation without any predefined assumption for the crack shape.

Additionally, in Figure 6b, the values of the two criteria proposed above in section 3.5 are compared throughout propagation. Both of them follow the same curve up to the 19th iteration. After that, the relative error continues to decrease towards a minimum very close to zero at the 25th iteration, while the absolute error decreases slightly to a minimum of 13% at the 21st iteration and then increases.

4.2 Evolution of the crack front

The evolution of the crack front from the initial straight shape to the two final semi-elliptical assumed shape is considered after both stabilization criteria.

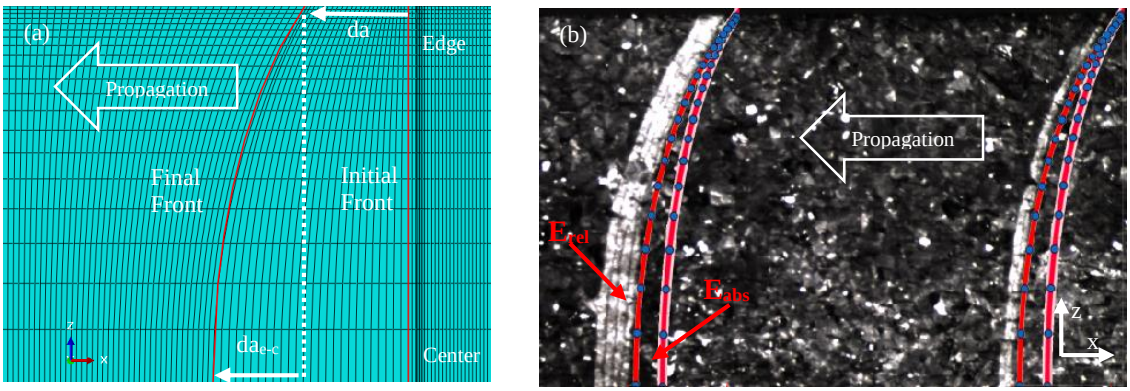

Figure 7 : ΔK = 12MPa√m, R = 0,1, initial straight front (a) Evolution of the numerical crack fronts (b) comparison between the numerical and the experimental fronts from [11]

Figure 7a allows to visualize the evolution of the crack fronts, in a half-thickness. On this figure, the crack advance on the edge da, as well as the difference between the crack advances at the center and at the edge d_{ae-c}, are defined. Figure 7b allows comparing the stabilized shape considering the two previous criteria to experimental observations [11] (the dark aspect corresponds to propagation in air, and light one to propagation under vacuum). It appears clearly that the front obtained with the relative criterion is really very close to the experimental one, whereas the one corresponding to the absolute one is a little bit less accurate.

Quantitative analysis is given in Table 2, where the values of da_{e-c} are given for experiments, the previous study [11] based on the calculation of the FIC based on the Shih and Asaro method based on an energetic approach and the two studied stabilization criteria. It appears clearly that, in these conditions of loading, $\Delta K = 12MPa\sqrt{m}$, $R = 0.1$, the method developed in this study, based on the calculation of FIC through stress fields, and with the relative stabilization criterion, allows to predict really accurately the crack front shape. This improvement in the results is due to the consideration of the plane stress conditions embedded in the stress field's method.

	Experiments[11]	Shih Asaro [11]	E_{rel}	E_{abs}
da_{e-c} (mm)	1.207	1.343	1.22	0.94
% error w.r.t experiments	-	11%	1%	22%

Table 2 : *Comparison of the values of da_{e-c} obtained numerically with experimental results, $\Delta K = 12MPa\sqrt{m}$, $R = 0.1$*

5 Conclusions and prospects

This paper presents a 3D numerical prediction of the crack front shape under fatigue loading in 304L stainless steel while considering the influence of the plasticity induced crack closure. A constant value of the applied stress intensity factor amplitude is considered (ΔK=12 MPa$\sqrt{m}$ and R=0.1). A straight initial crack front is considered in a CT specimen. Two parallel elastic and plastic simulations allow to calculate on each node of the crack front the local values of the effective stress intensity factor amplitudes, which are assumed to act as the driving force. The stress intensity factors are calculated through an interpolation of the opening stresses near the crack tip. Several steps are necessary to follow the crack propagation and to obtain stabilized semi-elliptical crack shapes, considering two stabilization methods.

The numerical results confirm that crack closure is far more important near the edge of the specimen, thus reducing the crack growth rate. The numerical curved crack fronts obtained are compared to experimental ones, and to the previous numerical results [11] using the Shih and Asaro method for the calculation of the stress intensity factors. The present method appears far much accurate.

Prospective work is already under progress to check both experimentally and numerically these results under other loading conditions, and also to use remeshing without assuming semi-elliptical crack fronts during propagation.

References

[1] F. V. Antunes, A. G. Chegini, R. Branco, and D. Camas, "A numerical study of plasticity induced crack closure under plane strain conditions," *Int. J. Fatigue*, vol. 71, pp. 75–86, Feb. 2015.

[2] R. G. Chermahini, B. Palmberg, and A. F. Blom, "Fatigue crack growth and closure behaviour of semicircular and semi-elliptical surface flaws," *Int. J. Fatigue*, vol. 15, no. 4, pp. 259–263, Jul. 1993.

[3] S. Roychowdhury and R. H. Dodds, "Three-dimensional effects on fatigue crack closure in the small-scale yielding regime – a finite element study," *Fatigue Fract. Eng. Mater. Struct.*, vol. 26, no. 8, pp. 663–673, Aug. 2003.

[4] J. D. Skinner and S. R. Daniewicz, "Simulation of plasticity-induced fatigue crack closure in part-through cracked geometries using finite element analysis," *Eng. Fract. Mech.*, vol. 69, no. 1, pp. 1–11, Jan. 2002.

[5] W. Elber, "The Significance of Fatigue Crack Closure," *Damage Toler. Aircr. Struct.*, vol. ASTM STP 486, pp. 230–242, Jun. 1971.

[6] K. Vor, C. Gardin, C. Sarrazin-Baudoux, and J. Petit, "Wake length and loading history effects on crack closure of through-thickness long and short cracks in 304L: Part I – Experiments," *Eng. Fract. Mech.*, vol. 99, pp. 266–277, Feb. 2013.

[7] K. Vor, C. Gardin, C. Sarrazin-Baudoux, and J. Petit, "Wake length and loading history effects on crack closure of through-thickness long and short cracks in 304L: Part II – 3D numerical simulation," *Eng. Fract. Mech.*, vol. 99, pp. 306–323, Feb. 2013.

[8] J. Toribio, J. C. Matos, B. González, and J. Escuadra, "Numerical modelling of cracking path in round bars subjected to cyclic tension and bending," *Int. J. Fatigue*, vol. 58, pp. 20–27, Jan. 2014.

[9] H. A. Richard, B. Schramm, and N.-H. Schirmeisen, "Cracks on Mixed Mode loading – Theories, experiments, simulations," *Int. J. Fatigue*, vol. 62, pp. 93–103, May 2014.

[10] B. R. Davis, P. A. Wawrzynek, and A. R. Ingraffea, "3-D simulation of arbitrary crack growth using an energy-based formulation – Part I: Planar growth," *Eng. Fract. Mech.*, vol. 115, pp. 204–220, Jan. 2014.

[11] S. Fiordalisi, "Modélisation tridimensionnelle de la fermeture induite par plasticité lors de la propagation d'une fissure de fatigue dans l'acier 304L," ISAE-ENSMA, Poitiers, 2014.

[12] J. D. Dougherty, J. Padovan, and T. S. Srivatsan, "Fatigue crack propagation and closure behavior of modified 1070 steel: Finite element study," *Eng. Fract. Mech.*, vol. 56, no. 2, pp. 189–212, Jan. 1997.

[13] X. B. Lin and R. A. Smith, "Finite element modelling of fatigue crack growth of surface cracked plates: Part I: The numerical technique," *Eng. Fract. Mech.*, vol. 63, no. 5, pp. 503–522, Jul. 1999.

[14] M. Arzaghi, C. Gardin, P. Chea, K. Vor, and C. Sarrazin-Baudoux, "Modélisation sous Abaqus de la fermeture de fissures courtes dans un acier inoxydable 304L," Congrès Français de Mécanique, Besançon, 2011.

[15] P. Yu and W. Guo, "An equivalent thickness conception for prediction of surface fatigue crack growth life and shape evolution," *Eng. Fract. Mech.*, vol. 93, pp. 65–74, Oct. 2012.

[16] C.-Y. Hou, "Simultaneous simulation of closure behavior and shape development of fatigue surface cracks," *Int. J. Fatigue*, vol. 30, no. 6, pp. 1036–1046, Jun. 2008.

[17] C.-Y. Hou, "Simulation of surface crack shape evolution using the finite element technique and considering the crack closure effects," *Int. J. Fatigue*, vol. 33, no. 5, pp. 719–726, May 2011.

[18] J. C. Newman and I. S. Raju, "An empirical stress-intensity factor equation for the surface crack," *Eng. Fract. Mech.*, vol. 15, no. 1, pp. 185–192, Jan. 1981.

[19] Z. Wu, "The shape of a surface crack in a plate based on a given stress intensity factor distribution," *Int. J. Press. Vessels Pip.*, vol. 83, no. 3, pp. 168–180, Mar. 2006.

[20] R. C. McClung, B. H. Thacker, and S. Roy, "Finite element visualization of fatigue crack closure in plane stress and plane strain," *Int. J. Fract.*, vol. 50, no. 1, pp. 27–49, Jul. 1991.